

STRESS ANALYSIS OF CERAMIC COATINGS UNDER SPHERICAL INDENTATION: INFLUENCE OF A METALLIC INTERLAYER

LE MINH QUY, TRAN ICH THINH

*Department of Mechanics of Materials and Structures,
Faculty of Mechanical Engineering, Hanoi University of Technology*

Abstract. Spherical indentation problems of ceramic coatings/metallic interlayer/ductile substrate were investigated numerically by axisymmetric FEA for two typical ceramic coatings with relatively high and low elastic modulus deposited on aluminum alloy and carbon steel. Various indenter radius-coating thickness ratios and interlayer thickness-coating thickness ratios were used in the modeling. Radial stress distributions were discussed in connection with model parameters. The results showed that the suitable metallic interlayer could improve resistance of ceramic coating systems through reducing the peak tensile radial stress on the surface and interface of ceramic coatings.

Key words: Finite element, ceramic coatings, indentation, interlayer

1. INTRODUCTION

It is well known that radial stresses occurred in ceramic coatings under spherical indentation are in general very high and cause surface and interface cracks. Therefore, radial stress pattern generated in the coatings under contact loading must be well understood. A recent review for the problems of spherical indentation into ceramic coatings can be found in [1, 2].

Our previous paper [1] studied the influence of a metallic interlayer on the plastic damage evolution in ceramic coating/interlayer/ductile substrate system under spherical indentation. This paper presents effects of metallic interlayer on radial stress distributions in ceramic coatings under spherical indentation. Spherical indentation problems of ceramic coatings/metallic inter-layer/ductile substrate are investigated numerically by an axisymmetric FEA for two typical ceramic coatings with relatively high and low elastic modulus deposited on aluminum alloy and carbon steel. Various indenter radius-coating thickness ratios and interlayer thickness-coating thickness ratios were used in the modeling. Radial stress distributions are discussed in connection with model parameters.

2. THE COMPUTATIONAL MODEL

2.1 Description of Materials

The computational model, materials properties, and geometric dimensions of the contact problem for fracture analysis in this paper are kept as those adopted in [1, 2].

Under spherical indentation, hard brittle ceramic coatings are assumed to behavior elastically. Metallic inter-layers and substrates can undergo plastic deformation with increasing indentation load according to Von Mises criterion [3]. The elastic-plastic behavior of metallic materials are modeled by a power law description as follows (see Fig. 1):

$$\begin{aligned}\sigma &= E\varepsilon, & (\sigma \leq Y), \\ \sigma &= K\varepsilon^n, & (\sigma \geq Y),\end{aligned}\tag{2.1}$$

where K is a strength coefficient, n is the strain-hardening exponent, Y is the initial yield stress, and ε_y is the corresponding yield strain. They have relation as follow

$$Y = E\varepsilon_y = K\varepsilon_y^n. \quad (2.2)$$

The total strain ε is a sum of elastic strain ε_e and plastic strain ε_p :

$$\varepsilon = \varepsilon_e + \varepsilon_p. \quad (2.3)$$

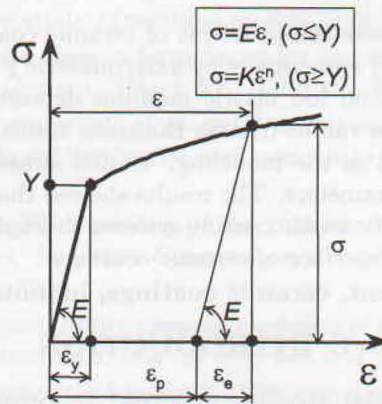


Fig. 1. The power-law elastic-plastic stress-strain behavior

Table 1 resumes the mechanical properties of modeled materials as those used in our previous paper [1].

Table 1 Mechanical properties of modeled materials

Materials	Elastic modulus (GPa)	Poisson's Ratio	Yield strength (GPa)	Strain hardening exponent
Steel	207	0.3	0.38	0
Aluminum alloy	70	0.3	0.140	0
Interlayer	110	0.3	0.680	0.25
Ceramic I	174	0.25	-	-
Ceramic II	480	0.2	-	-

2.2. Modeling Aspects and Finite Element Model

A Schematic representation of a ceramic coating under spherical indentation is presented in Fig. 2. Due to the symmetry, only one-half of the system is used in modeling as shown in Fig. 2b with respect to the $r - z$ coordinates system. Here, the origin of the coordinates corresponds to the point of intersection between the centerline of the structure and the surface of coating in the initial (un-deformed) configuration. The z -axis coincides to the centerline of the structure and expands downward. The r -axis, radial axis, belongs to the surface of coating and expands outward. Associated to this coordinate system, three normal stress components: σ_{rr} (radial stress), σ_{zz} (axial stress), $\sigma_{\theta\theta}$ (circumferential stress being perpendicular to $r - z$ plan) are described in Fig. 2c.

The spherical indentation of the coating/substrate was carried out by using the axisymmetric capacities of the MARC/MSC finite element code [4]. The indenter was modeled as a rigid sphere of radius R . The specimen was modeled as a large cylinder of height A and radius B ($A = B > 50a$, in all cases, where a is contact radius, see Fig. 2b). These dimensions were found to be large enough to approximate a semi-infinite half-space for indentations. This was evidenced by an insensitivity of calculated results to further increase in specimen size.

Frictionless roller boundary conditions were applied along the centerline and bottom. Outside surfaces were taken as free surfaces. The interaction between the rigid indenter and specimen was modeled by contact elements with no friction. The residual stresses were not taken account in the analysis. Large strain four-node elements were used.

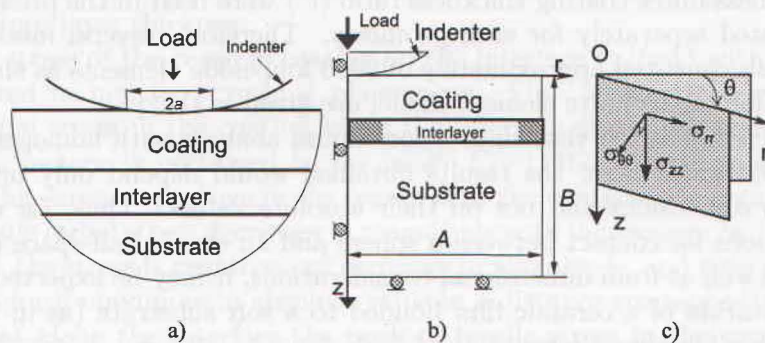


Fig. 2. Schematic representation of a ceramic coating under spherical indentation:
 a) contact zone with typical failure modes;
 b) axisymmetric model of the indenter and specimen with boundary conditions;
 c) three-dimensional coordinate system and normal stress notations.

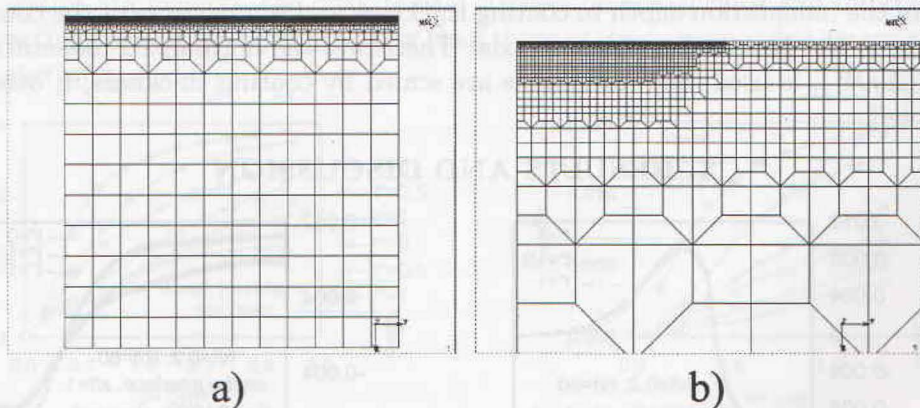


Fig. 3. Typical finite element mesh of a) half-space and b) zoom of the contact zone

To account properly for the high stress gradients under the indenter, estimate accurately of the peak tensile stress on the surface of ceramic coatings, and for an accurate detection the contact nodes, the mesh was made very fine locally near the contact area with an element size of $t/64$. The mesh was then gradually coarser outwards. The contact

was occurred at least with 45 elements at the first increment, and with approximately 200 elements at the maximum indentation load (final increment).

Both the force-controlled and displacement-controlled procedures were used in this work. The automatic depth increment scheme was used to determine the appropriate size of the load increments. For displacement controlled conditions, a maximum indentation depth, $h/t=0.2$, was used, then the indentation load P^* estimated automatically by the MARC/MSC finite element code [4] in each increment. Under load controlled conditions, the maximum normalized indentation loads, P^* , were calculated by the way that these maximum normalized indentation loads give an indentation depth, $h/t \sim 0.2$, for two ceramic coatings/steel substrate systems ($E_f=174\text{GPa}$ and 480GPa) without interlayer.

Several combinations of the indenter radius-coating thickness ratio (R/t) and of the interlayer thickness-outer coating thickness ratio (t^*) were used in the present study. The mesh was adapted separately for each geometry. Therefore, several meshes were used. The typical mesh consisted approximately of 9000 four-node elements as shown in Fig. 3.

The validation of the finite element model are given in [1, 2].

It should be emphasized that since a continuum analysis with homogeneous material properties is performed here, the results obtained would depend only on the ratios of different length dimensions and not on their absolute values. Thus, for example, from analytical solutions for contact between a sphere and an elastic half-space (see, e.g., K.L. Johnson [5]), as well as from dimensional considerations, it may be expected that the load P during indentation of a ceramic film bonded to a soft substrate (as in Fig. 2) would have the following functional form:

$$P = E_f R^2 f \left(\frac{h}{t}, \frac{t}{R}, \frac{E_s}{E_f}, \frac{Y_s}{E_s} \right), \quad \text{other parameter} \quad (2.4)$$

where E_f , E_s are the elastic modulus of ceramic film and substrate respectively. Y_s is yield stress of the substrate, h is indentation depth, other notations are shown in Fig. 2. h/t is the ratio of the indentation depth to coating thickness and is a measure of the compressive axial strain in the film at the indenter axis. Therefore, the normalized indentation load, $P^* = P / (E_f R^2)$, is used, and all lengths are scaled by coating thickness, t , otherwise it will be noted.

3. RESULTS AND DISCUSSION

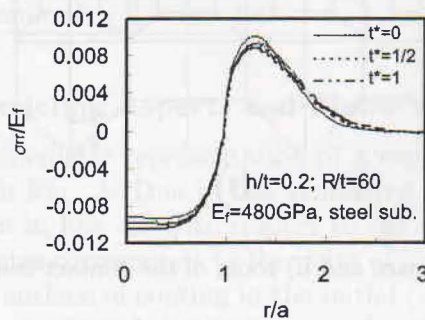


Fig. 4. Normalized radial stress distribution along the coating surface for $R/t=60$, $h/t=0.2$, and $E_f=480\text{GPa}$

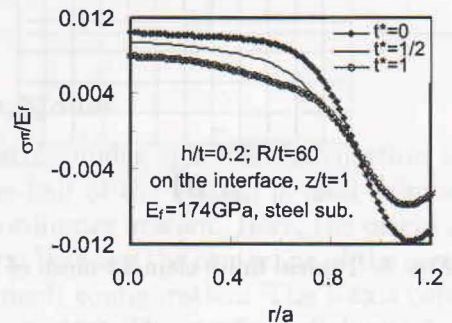


Fig. 5. Normalized radial stress in the coating along the interface for $R/t=60$, $h/t=0.2$, and $E_f=174\text{GPa}$

The results of our previous paper [1] showed that the interlayer can reduce effectively plastic damage zone size in the substrate and this effect of the interlayer is increased as increasing the interlayer thickness. By using FEA, effects of interlayer on radial stress distributions in ceramic coatings under spherical indentation are investigated here.

The evolution of normalized radial stress σ_{rr}/E_f along the film surface (i.e., $z=0$ in the un-deformed configuration) corresponding to $h/t=0.2$ for ceramic coatings deposited on the steel ($E_f=480\text{GPa}$) is shown in Fig. 4. The radial distance r is normalized by the contact radius a . The radial stress distributions plotted in Fig. 4 are typically Hertzian [5] and show a tensile peak just outside the contact zone. The magnitude of the tensile peak decreases with an increase in the thickness of the interlayer. These tensile stresses cause in general the cylindrical cracks located just outside the contact zone. It was found that from Fig. 4 the peak tensile stress on the ceramic coating surface is decreased as increasing the interlayer thickness.

The radial stress of the ceramic coating on the interface ($z/t=1$) with other material is strictly related to interface cracking phenomena. Fig. 5 shows the evolution of the normalized radial stress in the coating along the interface of ceramic coating with other material. This picture is pertained to the case: $E_f=174\text{GPa}$, steel substrate, $R/t=60$ and $h/t=0.2$. This stress is positive in the region near the contact axis ($r/a < 0.9$). In this region, the tensile radial stress decreases in magnitude with increasing r/a . Far the contact axis, $r/a > 0.9$, the stress is negative and increases in magnitude, and then decreases again after reached a local maximum in absolute value in a distance corresponding to $r/a \sim 1.1$. It is shown that along the interface the peak of tensile stress in the ceramic coating is obtained at the point of intersection between the interface ($z/t=1$) and the centerline ($r=0$ or the z -axis). It was also indicated that from Fig. 5 the peak tensile stress on the ceramic coating interface is decreased as increasing the interlayer thickness.

Fig. 6 and Fig. 7 present evolution of the peak tensile stresses versus indentation load for various combinations of ceramic coatings substrates and indenter radius-coating thickness ratios. In general, the peak tensile stresses on the surface and interface of the ceramic coatings with inter-layer are lower than those of the corresponded ceramic coatings without interlayer.

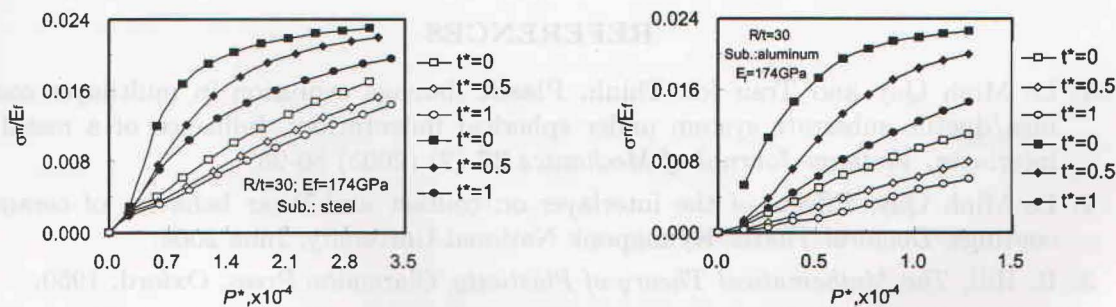


Fig. 6. Evolution of peak tensile stress on the surface (empty symbol) and on the interface (filled symbol) of the coating versus indentation load with $R/t=30$: a) steel and b) aluminum alloy

However, for low indentation loads, the inter-layers have a slight effect on decreasing the maximum tensile stress on the coating surfaces. This effect increases for high indentation loads. A thicker inter-layer provides larger reduction in the maximum tensile stress

on the coating surfaces. A large reduction in peak tensile stresses was found for ceramic coating deposited on the aluminum alloy.

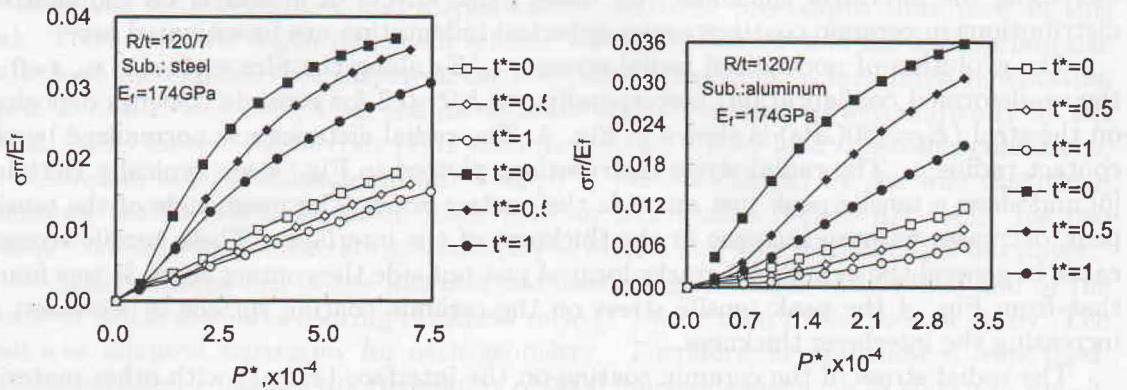


Fig. 7. Evolution of peak tensile stress on the surface (empty symbol) and on the interface (filled symbol) of the coating versus indentation load with $R/t=120/7$:
a) steel and b) aluminum alloy

5. CONCLUSIONS

Using the suitable metallic inter-layer, the ceramic coating/metallic inter-layer/substrate systems have the following advantages compared to ceramic coating systems without inter-layer:

The interlayer can reduce the peak tensile stresses on the surface and interface of ceramic coatings.

Effects of the interlayer increase as increasing the interlayer thickness.

This publication is completed with financial support from the National Basic Research Program in Natural Science.

REFERENCES

1. Le Minh Quy and Tran Ich Think, Plastic damage evolution in multilayer coatings/ductile substrate system under spherical indentation: Influence of a metallic interlayer, *Vietnam Journal of Mechanics* **27** (2) (2005) 86-95.
2. Le Minh Quy, Effects of the interlayer on contact and Wear behavior of ceramic coatings, *Doctoral Thesis*, Kyungpook National University, June 2004.
3. R. Hill, *The Mathematical Theory of Plasticity*, Clarendon Press, Oxford, 1950.
4. MARC. MSC, *Volume A: Theory and User Information*, MSC Software Corporation, 2000.
5. K. L. Johnson, *Contact Mechanics*, Cambridge University Press, 1985.

Received July 29, 2005

Revised October 26, 2005

PHÂN TÍCH ỨNG SUẤT CỦA LỚP MẠ GỐM CHỊU TẢI TRỌNG TIẾP XÚC CẦU: ẢNH HƯỞNG CỦA LỚP KIM LOẠI TRUNG GIAN

Bài toán tiếp xúc của kết cấu mạ gốm được khảo sát bằng phương pháp phần tử hữu hạn cho hai loại gốm có giá trị mô đun đàn hồi cao và thấp phủ trên nền hợp kim nhôm và thép các bon. Tỷ số giữa bán kính quả cầu tiếp xúc với chiều dày lớp mạ gốm và tỷ số giữa chiều dày lớp mạ gốm với chiều dày lớp trung gian được sử dụng như các tham số trong quá trình khảo sát. Sự phân bố của ứng suất hướng kính được nghiên cứu với các tham số khác nhau của mô hình. Kết quả chỉ ra rằng lớp mạ trung gian đã làm tăng độ bền của kết cấu mạ gốm vì nó đã làm giảm ứng suất kéo trên bề mặt và trên biên của lớp mạ gốm.